

Article

# Hydrogen Production from Glycerol Photoreforming on TiO<sub>2</sub>/HKUST-1 Composites: Effect of Preparation Method

Fabián M. Martínez <sup>1</sup>, Elim Albiter <sup>1</sup> , Salvador Alfaro <sup>1</sup> , Ana L. Luna <sup>2</sup>,  
Christophe Colbeau-Justin <sup>2</sup>, José M. Barrera-Andrade <sup>1</sup>, Hynd Remita <sup>2</sup> and  
Miguel A. Valenzuela <sup>1,\*</sup> 

<sup>1</sup> Laboratorio de Catálisis y Materiales, ESIQIE-Instituto Politécnico Nacional, México City 07738, Mexico; fmm003@eng.ucsd.edu (F.M.M.); ealbitere@ipn.mx (E.A.); salfaroh@ipn.mx (S.A.); jmanban@yahoo.com.mx (J.M.B.-A.)

<sup>2</sup> Laboratoire de Chimie Physique, CNRS UMR 8000 Université Paris-Sud, 91405 Orsay, France; aluna0786@gmail.com (A.L.L.); christophe.colbeau-justin@u-psud.fr (C.C.-J.); hynd.remita@u-psud.fr (H.R.)

\* Correspondence: mavalenz@ipn.mx; Tel.: +52-55-5729-6000 (ext. 55112)

Received: 12 March 2019; Accepted: 31 March 2019; Published: 4 April 2019



**Abstract:** Coupling metal-organic frameworks (MOFs) with inorganic semiconductors has been successfully tested in a variety of photocatalytic reactions. In this work we present the synthesis of TiO<sub>2</sub>/HKUST-1 composites by grinding, solvothermal, and chemical methods, using different TiO<sub>2</sub> loadings. These composites were used as photocatalysts for hydrogen production by the photoreforming of a glycerol-water mixture under simulated solar light. Several characterization techniques were employed, including X-ray diffraction (XRD), UV-Vis diffuse reflectance spectroscopy (DRS), infrared spectroscopy (FTIR), and time-resolved microwave conductivity (TRMC). A synergetic effect was observed with all TiO<sub>2</sub>/HKUST-1 composites (mass ratio TiO<sub>2</sub>/MOF 1:1), which presented higher photocatalytic activity than that of individual components. These results were explained in terms of an inhibition of the charge carrier (hole-electron) recombination reaction after photoexcitation, favoring the electron transfer from TiO<sub>2</sub> to the MOF and creating reversible Cu<sup>1+</sup>/Cu<sup>0</sup> entities useful for hydrogen production.

**Keywords:** hydrogen production; photocatalysis; TiO<sub>2</sub>-HKUST-1 composites; solar light

## 1. Introduction

Nowadays, one of the most important necessities of society is the use of natural renewable resources to produce energy, minimizing the use of fossil fuels and reducing the associated harmful pollution produced by their combustion. On the other hand, hydrogen is considered a good candidate as a green energy carrier because it produces null pollution during its combustion, and it can be obtained from renewable sources [1–3]. The use of hydrogen as an energy carrier has several benefits, such as the many different storage possibilities, its ability to be converted to other energy forms with ease and to be produced from water with near-zero emissions, and its high conversion efficiency [2]. However, there are also severe limitations for the widespread use of hydrogen, for example, as a fuel for transportation. If we are planning to use hydrogen-combustion and hydrogen-fuel-cell vehicles in the future, we must first resolve outstanding issues, such as the efficient and safe storage of hydrogen, creating a fueling infrastructure, and reducing its production costs [4]. Certainly, one possibility to reduce the production cost of hydrogen is the use of green energy sources. In this sense, hydrogen production using solar energy can be categorized as: (a) thermal, (b) photovoltaic, (c) bio-photolysis, and (c) photo-electrochemical [5]. Although most of the production methods involve renewable

sources, they are not well understood, and their development implies an increase in production costs and low global efficiency [2–5].

Photocatalytic hydrogen generation can be obtained mostly by two different approaches: (1) photocatalytic water splitting and (2) photocatalytic reforming of organics [6]. The first method relates to the capability of water to be reduced and oxidized by reacting with photogenerated electrons and positive holes, during semiconductor irradiation, in the presence of selected co-catalysts. The second approach is based on the ability of some organic species—namely, sacrificial agents—to donate electrons to the positive holes of the illuminated photocatalyst and be oxidized, generating proton ions, while photogenerated electrons reduce the latter to produce hydrogen in the presence of proper co-catalysts.

Glycerol is a sustainable compound that can be used for hydrogen production by photocatalytic reactions (photoreforming). Although this reaction has been studied extensively, the overall performance towards hydrogen evolution is low, and in many cases, a high photocatalytic activity is only achieved with UV-light irradiation. For this reason, the search for new materials, active and stable in the presence of sunlight, is of great interest [7–9].

Metal organic frameworks (MOFs) are obtained by the self-assembly of metal ions and organic ligands through the formation of covalent bonds or the presence of inter-molecular forces between them [10]. MOFs present a long-range periodic structure with good crystallinity, and MOF-based structures take some unique properties of both organic and inorganic porous materials. They exhibit several advantages such as a high surface area, tunable pore size, easy preparation, flexibility, and structural diversity [11]. CuMOF, also known as HKUST-1, copper-benzene-1,3,5-tricarboxylate (Cu-BTC), MOF-199 or Basolite® C300, was first assembled by Chui et al. [12] through the formation of coordination bonds between trimesic acid ( $H_3BTC$ ) and Cu ions [13].

MOFs have been investigated in many fields, such as sensing, drug delivery, sequestration, separation, molecular transport, electronics, bioreactors, optics, energy production, and catalysis, among others [14]. Applications in photocatalysis have been reported in the last decade, and since then, several articles and reviews have been published focusing on artificial photosynthesis (i.e., water splitting and  $CO_2$  photoreduction) [15,16], organic photosynthesis [17], and pollutants degradation [18,19].

Specifically, in solar-driven hydrogen evolution with the presence of a sacrificial electron donor, e.g., alcohols, most of the MOFs cannot be used as a stable and efficient photocatalyst for this application individually [20]. Certain modifications of the pristine MOF, including the decoration of the organic linker or metal center, combination with semiconductors, metal nanoparticles loading, decoration with reduced graphene oxide, sensitization, pyrolyzation, and incorporation with other functional materials, have been tested to increase their activity and stability under visible light [19,21].

Hybrid nanocomposites of semiconductors with MOFs have attracted increased attention because they improve charge transfer mechanisms with a lower charge recombination and more efficient light harvesting [22]. Hybrid nanocomposites based on  $TiO_2$  and HKUST-1 are exciting materials which could show synergic effects enhancing photocatalytic activity under visible light. Only a few investigations have reported the synthesis, structure, and properties (i.e., as photocatalysts in hydrogen production) of  $TiO_2$ /HKUST-1 nanocomposites [23–26]. Particularly, it has been reported that in these nanocomposites, HKUST-1 is transformed to Cu-Cu<sub>2</sub>O nanoparticles after calcination at 400 °C, presenting better rates of hydrogen production in comparison with Cu deposited on  $TiO_2$  by conventional methods [24]. There are contradictory results concerning the stability of HKUST-1. For example, when this MOF was used in aqueous media, it decomposed after 24 h of reaction [27]. However,  $TiO_2$ /HKUST-1 composites synthesized using ionic liquids as solvents showed high activity and stability during photo-oxidation/photoreduction reactions [28].

In this context, it would be very useful to know the role played by  $TiO_2$ -HKUST interactions on the activity and stability in glycerol photoreforming. Therefore,  $TiO_2$ /HKUST-1 composites were synthesized by employing three methods: the first composite was prepared by grinding the commercial

reagents, Aeroxide<sup>®</sup> TiO<sub>2</sub> P25 (Evonik, P25), and HKUST-1 (Basolite<sup>®</sup> C300). These composites were designated as TiO<sub>2</sub> P25/com-HKUST-1. The second one was formed by TiO<sub>2</sub> prepared by a solvothermal route in the presence of the commercial HKUST-1 (TiO<sub>2</sub>-ST/com-HKUST-1), and the third composite was prepared by synthesizing HKUST-1 by a chemical route in the presence of TiO<sub>2</sub> P25 (TiO<sub>2</sub> P25/syn-HKUST-1). Furthermore, the aim of the present work was focused on the effect of the preparation method of TiO<sub>2</sub>/HKUST-1 composites, as well as the mass ratio TiO<sub>2</sub>:MOF employed, on their photocatalytic properties for hydrogen production, using glycerol as a sacrificial agent.

## 2. Results

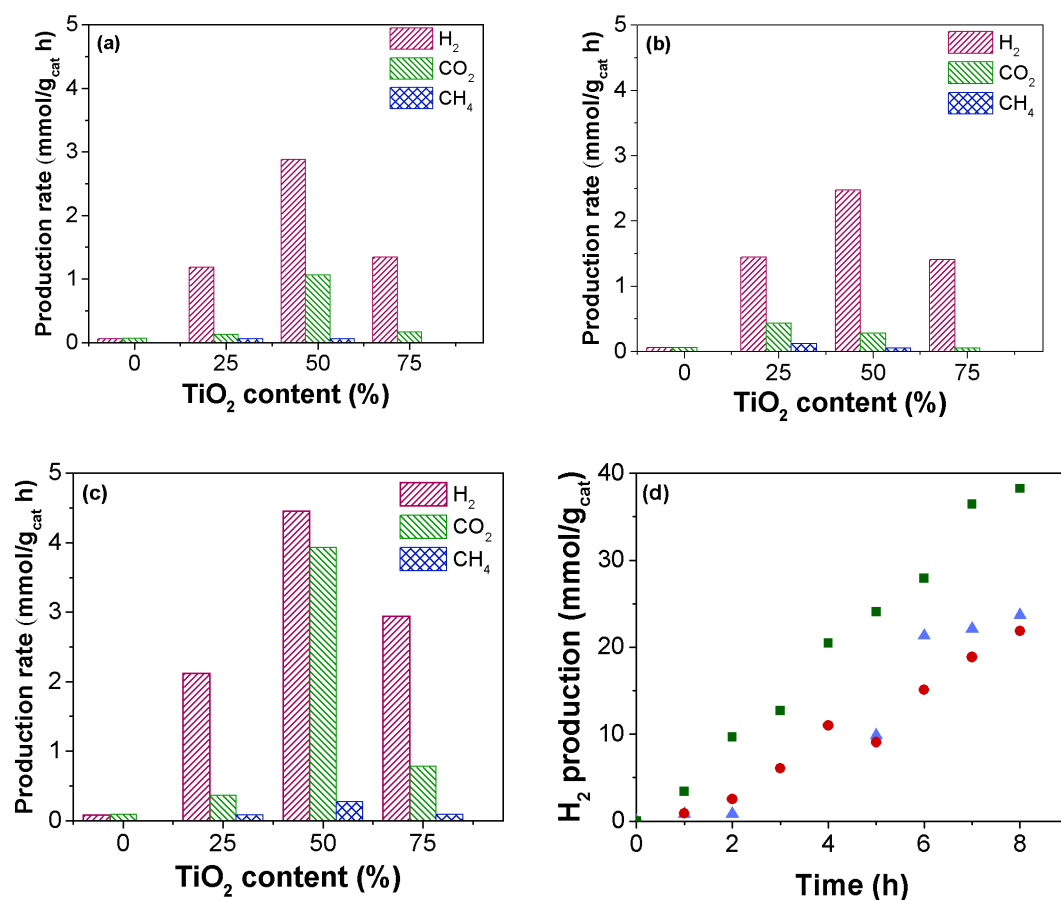
### 2.1. Photocatalytic Hydrogen Evolution

Due to the lack of studies regarding the effect of the optimal amount of TiO<sub>2</sub> that can be deposited on the HKUST-1, Figure 1 shows the photocatalytic hydrogen evolution rates as a function of TiO<sub>2</sub> content. All the experiments were conducted under similar operating conditions, and the H<sub>2</sub> production rate was estimated after 8 h of irradiation time. As can be observed, the results demonstrate a synergic photocatalytic activity between HKUST-1 and TiO<sub>2</sub>, and the best performance corresponds to the composites with 50 wt % TiO<sub>2</sub>. In the case of the catalyst prepared by grinding (50TiO<sub>2</sub> P25/com-HKUST-1) the production rate was 2.9 mmol × g<sup>-1</sup> × h<sup>-1</sup>, 2.4 mmol × g<sup>-1</sup> × h<sup>-1</sup> for the 50TiO<sub>2</sub>-ST/com-HKUST-1, and 4.5 mmol × g<sup>-1</sup> × h<sup>-1</sup> for the 50TiO<sub>2</sub> P25/syn-HKUST-1. Note that the photoactivity of the synthesized HKUST-1 and commercial HKUST-1 was insignificant, and as a comparison, the production rate shown by TiO<sub>2</sub> P25 was 1.1 mmol × g<sup>-1</sup> × h<sup>-1</sup>.

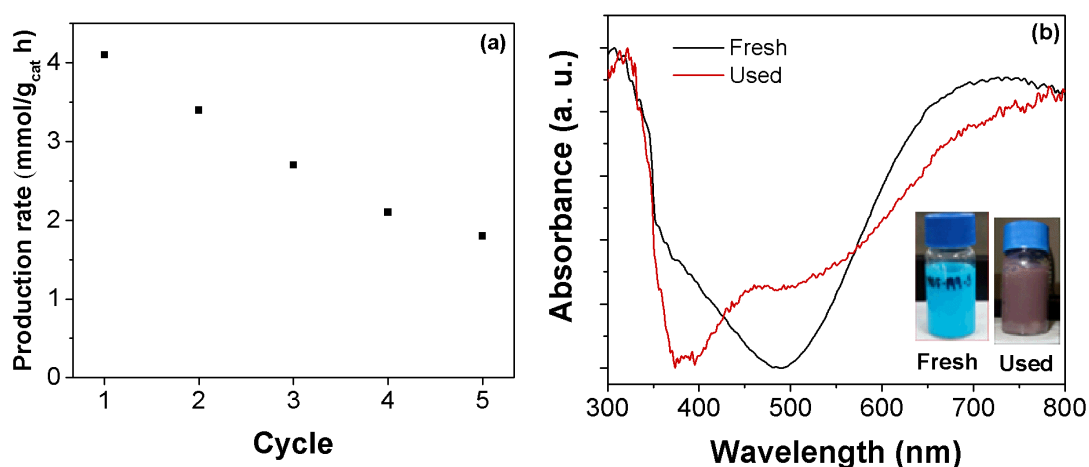
It is very important to highlight that during the reaction, there was a change in color in the photocatalysts from light blue (original composite color) to reddish brown (spent composite, see Figure 2b), which is indicative that the Cu<sup>2+</sup> originally present in the HKUST-1 was partially reduced towards Cu<sup>1+</sup> or Cu<sup>0</sup> [28,29]. This observation suggests that HKUST-1 assembled with Cu ions and benzene 1,3,5-tricarboxylate ligands (Cu-BTC) is an unstable material when irradiated in an aqueous medium, and functions as a precursor of Cu reduced species interacting with TiO<sub>2</sub>, as co-catalysts in the production of hydrogen. Note that the highest amounts of CO<sub>2</sub> and CH<sub>4</sub> were obtained with the 50TiO<sub>2</sub> P25/syn-HKUST-1 composite, which comes from the photocatalytic oxidation of an aqueous solution of glycerol. Indeed, it has been proposed that a secondary alcohol photoreforming can produce methane via β-hydride elimination, which could explain the origin of produced methane [30]. Figure 1d compares the amount of hydrogen produced as a function of the irradiation time for the prepared 50TiO<sub>2</sub>/HKUST-1 composites. Hydrogen production followed almost the same trend with the three photocatalysts. However, a higher photoactivity was observed with the 50TiO<sub>2</sub> P25/syn-HKUST-1 composite.

It is important to point out that only the 50TiO<sub>2</sub> P25/syn-HKUST-1 composite presented long-term activity, and it was evaluated in five cycles, under simulated solar light. Figure 2a shows the H<sub>2</sub> production rate reached during 8 h of reaction time in each cycle. It can be seen from the second cycle that the composite shows a reduction on the production rate, and in the fifth cycle the observed reduction was ca. 50% of the production rate observed in the first run. An explanation for this unfavorable behavior can be given in terms of a partial reduction of Cu<sup>2+</sup> contained in the original HKUST-1 by the photogenerated electrons in the TiO<sub>2</sub> conduction band, which was clearly demonstrated by the color change of the original HKUST-1 from light blue (original composite) to reddish brown (spent composite), as shown in Figure 2b. Furthermore, the zone attributed to the d-d spin allowed the transition of the Cu<sup>2+</sup> between 500–800 nm (discussed later), which was modified to a reddish-brown color, as is characteristic of Cu reduced species in the HKUST-1 structure [31]. Interestingly, after each reaction cycle and subsequent washing and purging of the reaction cell, the solid returned to the original light blue color of the composite. This means that the HKUST-1 structure was not completely destroyed, otherwise it would be forming the Cu<sup>1+</sup>-Cu<sup>2+</sup> MOF meta-stable phase with photocatalytic activity to reduce protons to hydrogen. This behavior was previously reported in other applications of

HKUST-1 [28,29,31,32] however, this is the first time that it has been observed in the photocatalytic hydrogen evolution reaction, which requires a systematic and thorough study.



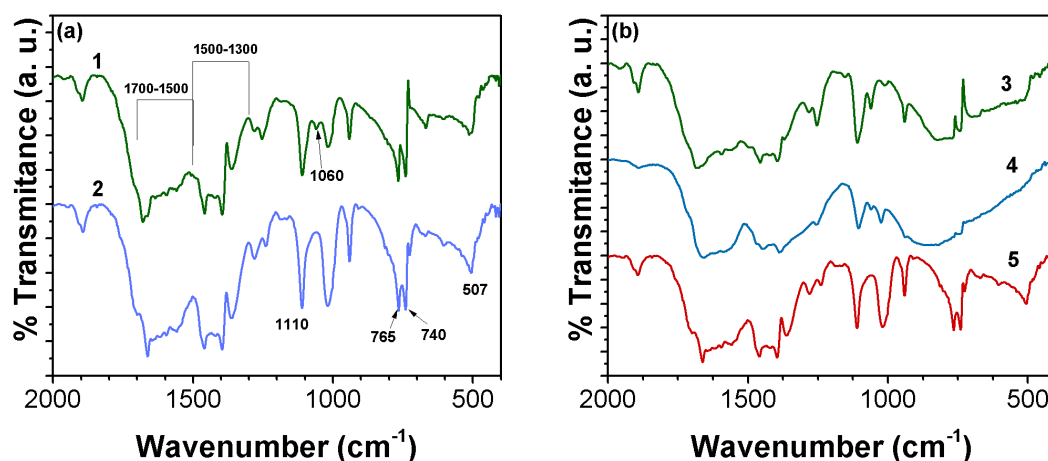
**Figure 1.** Effect of TiO<sub>2</sub> content on the H<sub>2</sub>, CO<sub>2</sub>, and CH<sub>4</sub> production rates of TiO<sub>2</sub>/HKUST-1 composites, after 8 h irradiation with simulated solar light with (a) TiO<sub>2</sub> P25/com-HKUST-1, (b) TiO<sub>2</sub>-ST/com-HKUST-1, and (c) TiO<sub>2</sub> P25/syn-HKUST-1 (d) Hydrogen evolution vs. time for TiO<sub>2</sub>/HKUST-1 composites: 50TiO<sub>2</sub> P25/com-HKUST-1 (▲), 50TiO<sub>2</sub>-ST/com-HKUST-1 (●), and 50TiO<sub>2</sub> P25/syn-HKUST-1 (■).



**Figure 2.** (a) Photocatalytic stability tests of 50TiO<sub>2</sub> P25/syn-HKUST-1, under simulated solar light, (b) UV-Vis diffuse reflectance spectra (DRS) of fresh and spent 50TiO<sub>2</sub> P25/syn-HKUST-1 composites.

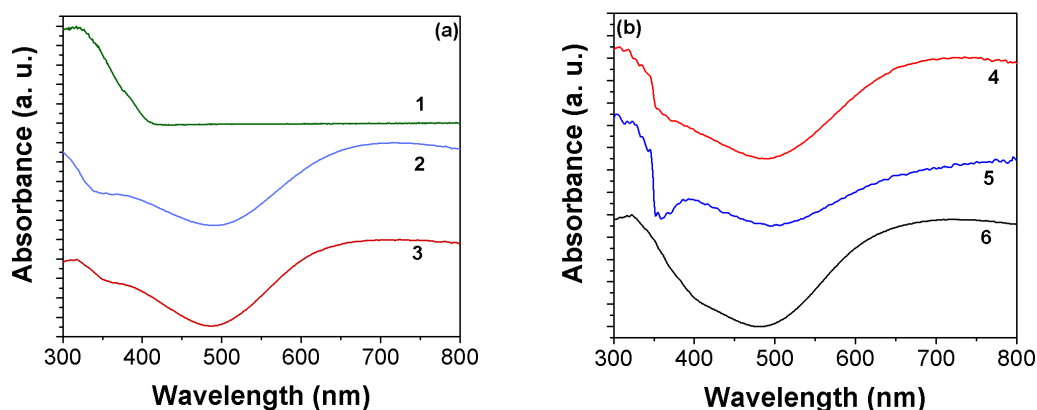
## 2.2. Characterization

Figure 3 shows the Fourier-transform infrared (FT-IR) spectra of com-HKUST-1, syn-HKUST-1, and TiO<sub>2</sub>/HKUST-1 composites. Clearly, the com-HKUST-1 and syn-HKUST-1 spectra are quite similar to those reported in previous works [33–35], which indicates that the method employed for the synthesis of syn-HKUST-1 was effective. In these spectra, several signals appeared in the range from 1300 to 1500 cm<sup>-1</sup> and from 1500 to 1700 cm<sup>-1</sup>, which are associated with the interactions between the carboxylate anion—in symmetric and asymmetric modes respectively—with the metal ion [34,35]. The signals indicated at 1110, 765, and 740 cm<sup>-1</sup> are associated with the C-H vibration modes in the aromatic ring [34]. The band at 1060 cm<sup>-1</sup> is attributed to the presence of copper coordinated *N,N*-dimethylformamide (DMF) molecules [33], and the band centered at 507 cm<sup>-1</sup> is assigned to the Cu-O stretching mode [35]. On the other hand, all the bands mentioned previously appeared in the spectrum of the 50TiO<sub>2</sub> P25/com-HKUST-1 composite, indicating a weak interaction between TiO<sub>2</sub> P25 and com-HKUST-1. In the case of the 50TiO<sub>2</sub>-ST/com-HKUST-1 and 50TiO<sub>2</sub> P25/syn-HKUST-1, the bands between 1300 and 1700 cm<sup>-1</sup> were less defined, and the signals at 507, 740, and 765 cm<sup>-1</sup> were replaced by a broad band (500–900 cm<sup>-1</sup>) in the case of TiO<sub>2</sub>-ST/com-HKUST-1 and two bands (500–700 and 765–830 cm<sup>-1</sup>) in the spectrum of 50TiO<sub>2</sub> P25/syn-HKUST-1. These last results could indicate that there is a chemical interaction between TiO<sub>2</sub> and HKUST-1 when either component is obtained by a chemical route.



**Figure 3.** Fourier-transform infrared (FT-IR) spectra of (a) syn-HKUST-1 (1), com-HKUST-1 (2) (b) 50TiO<sub>2</sub> P25/syn-HKUST-1 (3), 50TiO<sub>2</sub> ST/com-HKUST-1 (4), and 50TiO<sub>2</sub> P25/com-HKUST-1 (5).

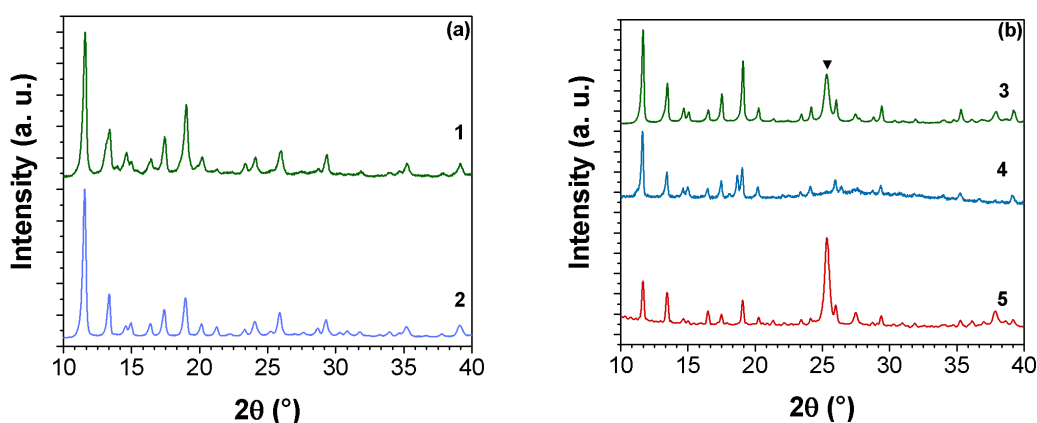
The optical properties of HKUST-1 and the TiO<sub>2</sub>/Cu MOFs composites were investigated by UV-Vis diffuse reflectance spectroscopy (DRS). As can be seen in Figure 4a, the as-prepared HKUST-1 sample and the commercial HKUST-1 showed a similar spectrum, exhibiting two characteristic absorption bands centered at 300 and 700 nm, similar values to those reported in the literature [36]. Note that one shoulder can also be detected at 375 nm. The first band located in the UV region is assigned to  $\pi$ - $\pi^*$  transitions of the ligands and the band in the visible zone is attributed to the d-d spin and allowed transition of the Cu<sup>2+</sup> [37]. The shoulder at 375 nm is ascribed to the ligand-to-metal charge transfer (LMCT), and the additional broad absorption band between 500 and 800 nm is assigned to the d-d spin and allowed transition of the Cu<sup>2+</sup> (d<sup>9</sup>) ions [37].



**Figure 4.** UV-Vis DRS spectra of (a) P25 (1), syn-HKUST-1 (2), com-HKUST-1 (3), and (b) TiO<sub>2</sub>/HKUST-1 composites: 50TiO<sub>2</sub> P25/com-HKUST-1 (4), 50TiO<sub>2</sub> ST/com-HKUST-1 (5), and 50TiO<sub>2</sub> P25/syn-HKUST-1 (6).

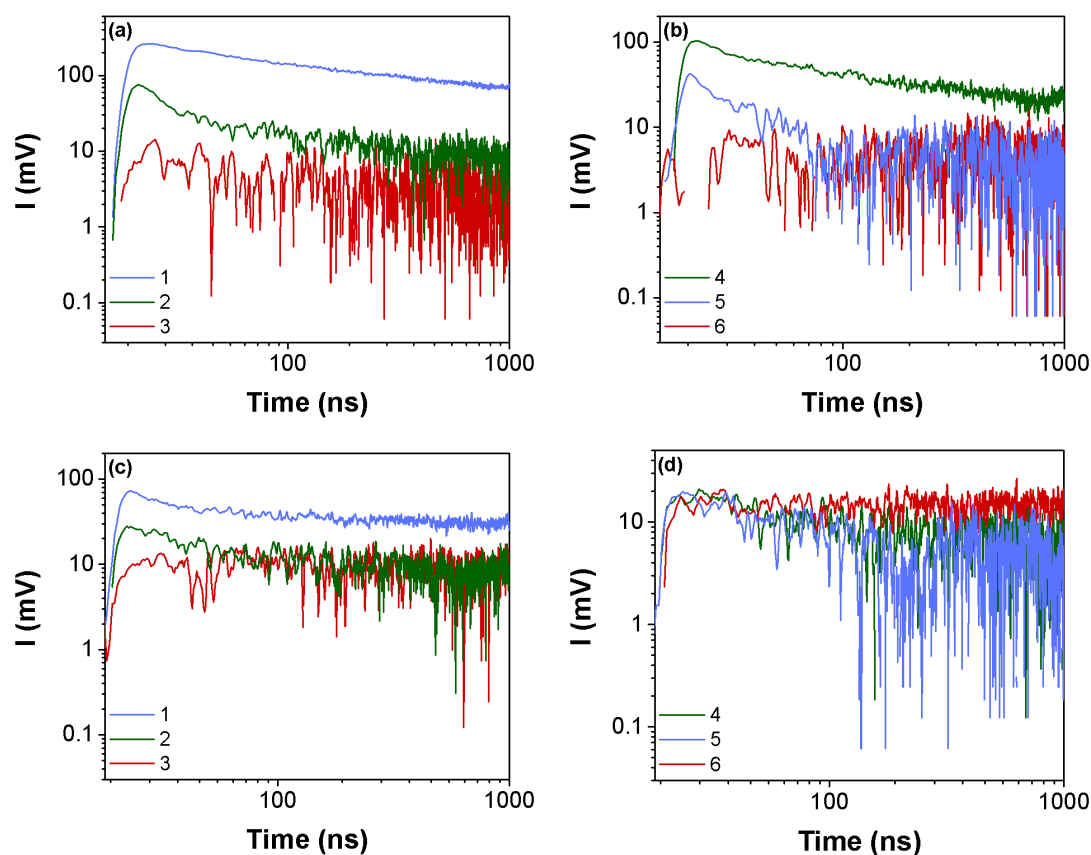
Figure 4b corresponds to the UV-Vis DRS spectra of the TiO<sub>2</sub>/HKUST-1 composites. In general, all composite photocatalysts showed similar absorption behavior to the pristine HKUST-1. However, it is worth noting a slight change of their absorption edge to the UV zone (350–400 nm), compared to those of commercial and synthesized HKUST-1 (Figure 4a), which can be related to the TiO<sub>2</sub>-HKUST-1 interaction. On the other hand, the slight differences in the 50TiO<sub>2</sub> ST/com-HKUST-1 composite spectrum (e.g., a lower absorption in the visible region) could be related to a shielding effect by TiO<sub>2</sub>, partially inhibiting the visible light absorption of the Cu<sup>2+</sup> ions in the HKUST-1 structure, because TiO<sub>2</sub>, in this particular composite, was grown in intimate contact with the commercial HKUST-1.

Figure 5a presents the X-ray diffraction (XRD) pattern of syn-HKUST-1, which is quite similar to the pattern of com-HKUST-1, showing the main reflections peaks at 11.6°, 13.4°, 17.4° and 19° [38,39]. These results prove that the HKUST-1 structure was successfully obtained using our described preparation method. XRD patterns of 50TiO<sub>2</sub> P25/com-HKUST-1, 50TiO<sub>2</sub> ST/com-HKUST-1, and 50TiO<sub>2</sub> P25/syn-HKUST-1 composites are shown in Figure 5b. These three samples displayed the same reflections described earlier, indicating that the HKUST-1 structure was preserved despite the preparation method used. Note that a higher crystallinity is observed in samples 50TiO<sub>2</sub> P25/com-HKUST-1 and 50TiO<sub>2</sub> P25/syn-HKUST-1 in comparison with sample 50TiO<sub>2</sub> ST/com-HKUST-1, which means that a poor crystallization of TiO<sub>2</sub> occurred due to the low synthesis temperature (i.e., 100 °C) compared to that reported in the literature, above 150 °C under solvothermal process [40].



**Figure 5.** X-ray diffraction patterns of (a) as-sensitized HKUST-1 (1), commercial HKUST-1 (2), and (b) 50TiO<sub>2</sub> P25/com-HKUST-1 (3), 50TiO<sub>2</sub> ST/com-HKUST-1 (4), and 50TiO<sub>2</sub> P25/syn-HKUST-1 (5). ▼ denotes the peak corresponding to TiO<sub>2</sub> anatase.

Figure 6a compares the time-resolved microwave conductivity (TRMC) profiles of TiO<sub>2</sub> P25, syn-HKUST-1, and com-HKUST-1, obtained under a wavelength excitation of 355 nm. The highest signal was exhibited by TiO<sub>2</sub> P25, which also presented a long-time decay. It is worth noting that syn-HKUST-1 showed a TRMC signal because it behaves like a semiconductor material; however, it decays faster than TiO<sub>2</sub> P25, revealing a short lifetime of photogenerated electrons. Surprisingly, com-HKUST-1, which presented very similar structure and light absorption (see Figure 4a) to those of syn-HKUST-1, displayed a much lower TRMC signal, revealing a great difficulty in executing the charge separation after irradiation with UV light of 355 nm.



**Figure 6.** Time-resolved microwave conductivity (TRMC) transient signal of (a,c) P25 (1), syn-HKUST-1 (2), com-HKUST-1 (3) (b,d) TiO<sub>2</sub>/HKUST-1 composites: 50TiO<sub>2</sub> P25/com-HKUST-1 (4), 50TiO<sub>2</sub> ST/com-HKUST-1 (5), and 50TiO<sub>2</sub> P25/syn-HKUST-1 (6). The excitation wavelengths were 355 nm (a,b) and 410 nm (c,d).

On the other hand, by analyzing the TRMC signals of the composites in Figure 6b, the sample prepared by grinding (sample 4) displayed a decay profile quite similar than that obtained with TiO<sub>2</sub> P25, indicating that the charge carrier dynamics are mainly due to the TiO<sub>2</sub> P25 contribution. Unexpectedly, the 50TiO<sub>2</sub> ST/com-HKUST-1 (sample 5) presented a TRMC signal with an  $I_{\max}$  value slightly smaller than that of the grinding composite (sample 4), clearly showing a charge carrier separation, but with a short time decay. The decay signal abruptly becomes highly noisy after 70 ns, denoting a charge carrier recombination or electron transfer from TiO<sub>2</sub> to HKUST-1. The 50TiO<sub>2</sub> ST/com-HKUST-1 (sample 6) did not display a clear TRMC signal, similar to that shown by the com-HKUST-1 (Figure 6a), which can be connected with the XRD results, meaning that TiO<sub>2</sub> was poorly crystallized.

As simulated solar light is being used in the photocatalytic evaluation, it is interesting to see the TRMC signals of the materials under 410 nm excitation. As can be seen in Figure 6c, TiO<sub>2</sub> P25, com-HKUST-1 and syn-HKUST-1MOFs presented similar behaviors to those presented under 355 nm

excitation, but all the samples showed a lower  $I_{\max}$  value. The  $\text{TiO}_2$  P25 signal can be attributed to the presence of rutile, which has a bandgap of 3.0 eV, making possible the generation of electron-hole pairs under visible-light irradiation. All the composites shown in Figure 6d exhibited a small TRMC signal, which means that they have the capacity to generate electron-hole pairs under 410 nm excitation.

### 3. Discussion

The above results suggest that the photocatalytic performance of  $\text{TiO}_2$  is improved by the incorporation of HKUST-1, forming a semiconductor-MOF composite regardless the preparation method. Nonetheless, the integration of HKUST-1 with  $\text{TiO}_2$  P25 ( $\text{TiO}_2$  P25/syn-HKUST-1) by a chemical method showed greater photocatalytic activity and stability compared with to grinding ( $\text{TiO}_2$  P25/com-HKUST-1) or the  $\text{TiO}_2$ -ST/com-HKUST-1. At first glance, the greater photocatalytic activity shown by the composites in comparison with  $\text{TiO}_2$  P25 or HKUST-1 is explained by the synergy between the semiconductor and the MOF, inhibiting electron-hole recombination. This cooperative behavior implied the partial reduction of the  $\text{Cu}^{2+}$  contained in the MOF, forming  $\text{Cu}^{1+}$  species which absorb visible light and could contribute to the proton reduction, as shown in Figure 7. The creation of reversible  $\text{Cu}^{1+}/\text{Cu}^{2+}$  entities in the composite was attributed to the electron transfer from P25 to HKUST-1 generating in situ species, i.e.,  $\text{Cu}^{1+}$ - $\text{Cu}^{2+}$  MOF, giving rise to improved hydrogen production.

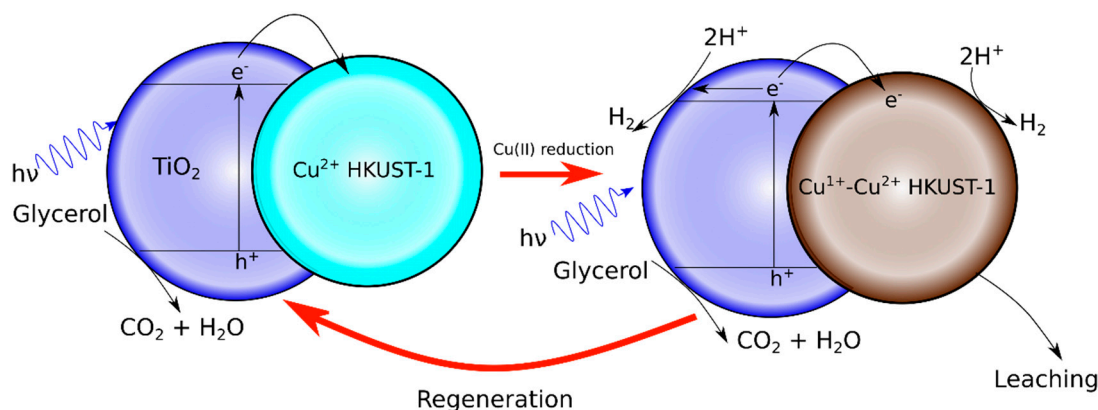


**Figure 7.** Proposed photocatalytic mechanism of glycerol photoreforming with the  $\text{TiO}_2$  P25/syn-HKUST-1 under solar light irradiation.

Furthermore, it was found that the higher photoactivity and stability shown by the  $\text{TiO}_2$  P25/syn-HKUST-1 can also be related to a strong interaction between the two components, which was not seen with the other two composites prepared by grinding or mixing poor crystallized  $\text{TiO}_2$  with commercial HKUST-1.

## 4. Materials and Methods

### 4.1. Materials

Copper (II) acetate monohydrate ( $\text{Cu}(\text{OAc})_2\text{H}_2\text{O}$ ), trimesic acid ( $\text{H}_3\text{BTC}$ ), *N,N*-dimethylformamide (DMF), Triethylamine ( $\text{Et}_3\text{N}$ ), and Titanium (IV) isopropoxide were purchased from Sigma-Aldrich (St. Louis, MO, USA), Ethanol ( $\text{EtOH}$ ) and ammonium hydroxide 30% were purchased from Panreac Chemicals (Chicago, IL, USA), and deionized water ( $\text{H}_2\text{O}$ ), Aeroxide<sup>®</sup>  $\text{TiO}_2$  P25 (Degussa), and Basolite<sup>®</sup> C300 (Sigma-Aldrich) were used as reference materials without further purification.

## 4.2. Preparation Methods

### 4.2.1. Grinding (TiO<sub>2</sub> P25/com-HKUST-1)

The composites were prepared by grinding the TiO<sub>2</sub> P25 and commercial HKUST-1 powders by hand in an agate mortar until a homogeneous light blue color was obtained. Five composites were prepared with a TiO<sub>2</sub> content of 25, 50 and 75 wt %.

### 4.2.2. TiO<sub>2</sub> Solvothermal Deposition on Commercial HKUST-1 (TiO<sub>2</sub>-ST/com-HKUST-1)

TiO<sub>2</sub> was prepared by mixing 1.14 mL of titanium (IV) isopropoxide with 100 mL of anhydrous ethanol and sonicating this for 5 min. Then, under vigorous magnetic stirring, concentrated nitric acid (70% *v/v*) was added drop by drop to get a pH around 1. The solution was diluted with 10 mL of distilled water, and 8 mL of ammonium hydroxide was added as a precipitating agent. Subsequently, a given amount of commercial HKUST-1 was added to the suspension under vigorous stirring. The resultant suspension was placed in a homemade PTFE-lined autoclave and sealed hermetically, and then introduced into a convective furnace (Fisher Scientific, Pittsburgh PA, USA) at 100 °C for 24 h. The composite formed was recovered and washed five times with a mixture of DMF/EtOH/H<sub>2</sub>O (molar ratio of 1:1:1) to eliminate the residues of any organic compound. Then, the product was dried at 50 °C for 5 h. The solid was ground in an agate mortar and sieved using a US 80 mesh to get a homogeneous particle size. Three composites were prepared by this method with a nominal TiO<sub>2</sub> content of 25, 50, and 75 wt %.

### 4.2.3. TiO<sub>2</sub> P25 Incorporation During HKUST-1 Synthesis (TiO<sub>2</sub> P25/syn-HKUST-1)

The synthesis route of synthesized HKUST-1 mainly followed the procedure reported by Tranchemontagne et al. [41] with some modifications, such as the integration of the TiO<sub>2</sub> P25 during the preparation of precursor solution. First, two solutions were prepared: one solution containing 100 mg of trimesic acid (H<sub>3</sub>BTC) dissolved in 6 mL of a mixture of DMF/EtOH/H<sub>2</sub>O with a molar ratio (1:1:1), and a second solution contained 200 mg of Cu(OAc)<sub>2</sub> × H<sub>2</sub>O dissolved in 6 mL of the solvent DMF/EtOH/H<sub>2</sub>O. Both solutions were mixed under magnetic stirring to get a homogeneous solution. Then, 0.2 mL of Et<sub>3</sub>N was added drop by drop as an oxidant agent to the reaction mixture under magnetic stirring. After that, a given quantity of TiO<sub>2</sub> P25 (25, 50 and 75 wt %) was added to the MOFs precursor solution. This suspension was kept under magnetic stirring for 24 h, and the powder was obtained by centrifugation. The solid was washed five times with 5 mL of DMF to eliminate the residues of any organic compound, and finally, the solid was dried—at 50 °C for 5 h—milled and sieved to get a homogeneous particle size.

## 4.3. Characterization Techniques

All composites were characterized by several techniques. X-ray diffraction patterns were recorded on a Siemens D-5000 diffractometer (Munich, Germany), with a copper anode and Cu-K $\alpha$  radiation over a 2 theta range of 10–80° using a step size of 4 °/min. FTIR and UV-Vis spectra of powder samples were respectively obtained using a Nicolet system (Nexus 470, Thermo Fisher Scientific, Waltham, MA, USA) (with KBr pellet samples) and a GBC spectrophotometer (Cintra 20, GBC Scientific, Hampshire, IL, USA), respectively.

The dynamics of the charge carriers in the photocatalysts were studied by the TRMC technique. The TRMC set-up consists of two main components: (1) a pulse light source, which has the objective to photo-excite the samples and (2) microwave source. A Gunn diode of K $\alpha$  band at 30 GHz was used to generate the incident microwaves. A tunable laser in the range between 220 and 2000 nm (NT342B; EKSPLA, Vilnius, Lithuania) was used as a light source. It was equipped with an optical parametric oscillator (OPO). The laser delivered 8 ns FWHM pulses with a frequency of 10 Hz. The selected excitation wavelengths were 355 and 410 nm, with a light energy density of 747.6  $\mu\text{J} \times \text{cm}^{-2}$  and 2.6  $\text{mJ} \times \text{cm}^{-2}$ , respectively.

#### 4.4. Photocatalytic H<sub>2</sub> Evolution

The composite powders were evaluated in the hydrogen production reaction using a glycerol-water solution with a volumetric ratio glycerol/water = 1:9. The photocatalytic reaction was carried out in a 25 mL glass cell. The composites (1 g/L) and the glycerol-water mixture was placed in the cell and mixed to form a homogeneous suspension, and then purged with nitrogen to eliminate all dissolved oxygen. Before irradiation, the reaction cell was maintained under stirring for one hour for adsorption/desorption equilibration and then irradiated with a solar simulator (Model 9600, 150 W; Newport Corporation, Irvine, CA, USA) for 8 h or 24 h. The gas mixture (H<sub>2</sub>, CO<sub>2</sub>, CH<sub>4</sub>) produced during the reaction was analyzed in a Perkin–Elmer Gas Chromatograph (Autosystem XL, Waltham, MA, USA).

## 5. Conclusions

A series of TiO<sub>2</sub>/HKUST-1 composites were successfully prepared using grinding, solvothermal, and chemical methods. All composites showed a higher photocatalytic activity than the individual components, particularly those containing a TiO<sub>2</sub>/HKUST-1 weight ratio of 1:1. These results demonstrated the effect of the synthesis method of composites on photocatalytic activity and stability. The best performance was obtained with the composite prepared by a chemical route, i.e., the synthesis of HKUST-1 in the presence of TiO<sub>2</sub> P25, leading to a strong interaction between the two components. The higher photocatalytic performance of the composites, compared with TiO<sub>2</sub> or HKUST-1, was explained regarding a synergy between the semiconductor and the HKUST-1, inhibiting electron-hole recombination. There was experimental evidence of the reversible partial reduction of Cu<sup>2+</sup> towards the Cu<sup>1+</sup>-Cu<sup>0</sup> entities contained in HKUST-1, which could indicate the in situ formation of highly active HKUST-1 co-catalysts, improving the photocatalytic activity.

**Author Contributions:** Conceptualization, S.A., and M.A.V.; investigation, F.M.M., and A.L.L.; methodology, C.C.-J., M.A.V., and H.R.; writing—original draft preparation, M.A.V., and S.A.; writing—review and editing, E.A., and J.M.B.-A.

**Funding:** This research was sponsored by “Consejo Nacional de Ciencia y Tecnología” México (Project No. 153356), and “Instituto Politécnico Nacional” (Projects SIP 20194976 and SIP 20196347).

**Acknowledgments:** M.V. and H.R. acknowledge Université Paris-Saclay for the financial support through the Chaire Jean d’Alembert program and the IRS MOMENTOM (Initiative de Recherche Stratégique).

**Conflicts of Interest:** The authors declare no conflict of interest.

## References

1. Andrews, J.; Shabani, B. Re-envisioning the role of hydrogen in a sustainable energy economy. *Int. J. Hydrog. Energy* **2012**, *37*, 1184–1203. [[CrossRef](#)]
2. Dincer, I.; Acar, C. Review and evaluation of hydrogen production methods for better sustainability. *Int. J. Hydrog. Energy* **2015**, *40*, 11094–11111. [[CrossRef](#)]
3. Dodds, P.E.; Staffell, I.; Hawkes, A.D.; Li, F.; Grünewald, P.; McDowall, W.; Ekins, P. Hydrogen and fuel cell technologies for heating: A review. *Int. J. Hydrog. Energy* **2015**, *40*, 2065–2083. [[CrossRef](#)]
4. Liao, C.-H.; Huang, C.-W.; Wu, J.C.S. Hydrogen Production from Semiconductor-based Photocatalysis via Water Splitting. *Catalysts* **2012**, *2*, 490–516. [[CrossRef](#)]
5. Bozoglan, E.; Midilli, A.; Hepbasli, A. Sustainable assessment of solar hydrogen production techniques. *Energy* **2012**, *46*, 85–93. [[CrossRef](#)]
6. Christoforidis, K.C.; Fornasiero, P. Photocatalytic Hydrogen Production: A Rift into the Future Energy Supply. *ChemCatChem* **2017**, *9*, 1523–1544. [[CrossRef](#)]
7. Babu, V.J.; Vempati, S.; Uyar, T.; Ramakrishna, S. Review of one-dimensional and two-dimensional nanostructured materials for hydrogen generation. *Phys. Chem. Chem. Phys.* **2015**, *17*, 2960–2986. [[CrossRef](#)] [[PubMed](#)]
8. Guo, L.; Jing, D.; Liu, M.; Chen, Y.; Shen, S.; Shi, J.; Zhang, K. Functionalized nanostructures for enhanced photocatalytic performance under solar light. *Beilstein J. Nanotechnol.* **2014**, *5*, 994–1004. [[CrossRef](#)]

9. Kumar, S.; Kumar, A.; Bahuguna, A.; Sharma, V.; Krishnan, V. Two-dimensional carbon-based nanocomposites for photocatalytic energy generation and environmental remediation applications. *Beilstein J. Nanotechnol.* **2017**, *8*, 1571–1600. [[CrossRef](#)]
10. Rowsell, J.L.C.; Yaghi, O.M. Metal–organic frameworks: A new class of porous materials. *Microporous Mesoporous Mater.* **2004**, *73*, 3–14. [[CrossRef](#)]
11. Nguyen, L.T.L.; Nguyen, T.T.; Nguyen, K.D.; Phan, N.T.S. Metal–organic framework MOF-199 as an efficient heterogeneous catalyst for the aza-Michael reaction. *Appl. Catal. Gen.* **2012**, *425–426*, 44–52. [[CrossRef](#)]
12. Chui, S.S.-Y.; Lo, S.M.-F.; Charmant, J.P.H.; Orpen, A.G.; Williams, I.D. A Chemically Functionalizable Nanoporous Material [Cu<sub>3</sub>(TMA)<sub>2</sub>(H<sub>2</sub>O)<sub>3</sub>]<sub>n</sub>. *Science* **1999**, *283*, 1148–1150. [[CrossRef](#)]
13. Prestipino, C.; Regli, L.; Vitillo, J.G.; Bonino, F.; Damin, A.; Lamberti, C.; Zecchina, A.; Solari, P.L.; Kongshaug, K.O.; Bordiga, S. Local Structure of Framework Cu(II) in HKUST-1 Metallorganic Framework: Spectroscopic Characterization upon Activation and Interaction with Adsorbates. *Chem. Mater.* **2006**, *18*, 1337–1346. [[CrossRef](#)]
14. Kumar, P.; Vellingiri, K.; Kim, K.-H.; Brown, R.J.C.; Manos, M.J. Modern progress in metal-organic frameworks and their composites for diverse applications. *Microporous Mesoporous Mater.* **2017**, *253*, 251–265. [[CrossRef](#)]
15. Wen, M.; Mori, K.; Kuwahara, Y.; An, T.; Yamashita, H. Design and architecture of metal organic frameworks for visible light enhanced hydrogen production. *Appl. Catal. B Environ.* **2017**, *218*, 555–569. [[CrossRef](#)]
16. Zhang, T.; Lin, W. Metal–organic frameworks for artificial photosynthesis and photocatalysis. *Chem. Soc. Rev.* **2014**, *43*, 5982–5993. [[CrossRef](#)] [[PubMed](#)]
17. Deng, X.; Li, Z.; García, H. Visible Light Induced Organic Transformations Using Metal–Organic-Frameworks (MOFs). *Chem. Eur. J.* **2017**, *23*, 11189–11209. [[CrossRef](#)]
18. Wang, C.-C.; Li, J.-R.; Lv, X.-L.; Zhang, Y.-Q.; Guo, G. Photocatalytic organic pollutants degradation in metal–organic frameworks. *Energy Environ. Sci.* **2014**, *7*, 2831–2867. [[CrossRef](#)]
19. Dias, E.M.; Petit, C. Towards the use of metal–organic frameworks for water reuse: a review of the recent advances in the field of organic pollutants removal and degradation and the next steps in the field. *J. Mater. Chem. A* **2015**, *3*, 22484–22506. [[CrossRef](#)]
20. Fang, Y.; Ma, Y.; Zheng, M.; Yang, P.; Asiri, A.M.; Wang, X. Metal–organic frameworks for solar energy conversion by photoredox catalysis. *Coord. Chem. Rev.* **2018**, *373*, 83–115. [[CrossRef](#)]
21. Qiu, J.; Zhang, X.; Feng, Y.; Zhang, X.; Wang, H.; Yao, J. Modified metal-organic frameworks as photocatalysts. *Appl. Catal. B Environ.* **2018**, *231*, 317–342. [[CrossRef](#)]
22. Aguilera-Sigalat, J.; Bradshaw, D. Synthesis and applications of metal-organic framework–quantum dot (QD@MOF) composites. *Coord. Chem. Rev.* **2016**, *307*, 267–291. [[CrossRef](#)]
23. Li, R.; Hu, J.; Deng, M.; Wang, H.; Wang, X.; Hu, Y.; Jiang, H.-L.; Jiang, J.; Zhang, Q.; Xie, Y.; et al. Integration of an Inorganic Semiconductor with a Metal–Organic Framework: A Platform for Enhanced Gaseous Photocatalytic Reactions. *Adv. Mater.* **2014**, *26*, 4783–4788. [[CrossRef](#)]
24. Binh, N.T.; Thu, P.T.; Le, N.T.H.; Tien, D.M.; Khuyen, H.T.; Giang, L.T.K.; Huong, N.T.; Lam, T.D. Study on preparation and properties of a novel photo-catalytic material based on copper-centred metal–organic frameworks (Cu–MOF) and titanium dioxide. *Int. J. Nanotechnol.* **2015**, *12*, 447–455. [[CrossRef](#)]
25. Abedi, S.; Morsali, A. Ordered Mesoporous Metal–Organic Frameworks Incorporated with Amorphous TiO<sub>2</sub> As Photocatalyst for Selective Aerobic Oxidation in Sunlight Irradiation. *ACS Catal.* **2014**, *4*, 1398–1403. [[CrossRef](#)]
26. Li, R.; Wu, S.; Wan, X.; Xu, H.; Xiong, Y. Cu/TiO<sub>2</sub> octahedral-shell photocatalysts derived from metal–organic framework@semiconductor hybrid structures. *Inorg. Chem. Front.* **2016**, *3*, 104–110. [[CrossRef](#)]
27. Canivet, J.; Fateeva, A.; Guo, Y.; Coasne, B.; Farrusseng, D. Water adsorption in MOFs: Fundamentals and applications. *Chem. Soc. Rev.* **2014**, *43*, 5594–5617. [[CrossRef](#)]
28. Chen, C.; Wu, T.; Yang, D.; Zhang, P.; Liu, H.; Yang, Y.; Yang, G.; Han, B. Catalysis of photooxidation reactions through transformation between Cu<sup>2+</sup> and Cu<sup>+</sup> in TiO<sub>2</sub>–Cu–MOF composites. *Chem. Commun.* **2018**, *54*, 5984–5987. [[CrossRef](#)]
29. Ahmed, A.; Robertson, C.M.; Steiner, A.; Whittles, T.; Ho, A.; Dhanak, V.; Zhang, H. Cu(I)Cu(II)BTC, a microporous mixed-valence MOF via reduction of HKUST-1. *RSC Adv.* **2016**, *6*, 8902–8905. [[CrossRef](#)]
30. Bahruji, H.; Bowker, M.; Davies, P.R.; Al-Mazroai, L.S.; Dickinson, A.; Greaves, J.; James, D.; Millard, L.; Pedrono, F. Sustainable H<sub>2</sub> gas production by photocatalysis. *J. Photochem. Photobiol. Chem.* **2010**, *216*, 115–118. [[CrossRef](#)]

31. Szanyi, J.; Daturi, M.; Clet, G.; Baer, D.R.; Peden, C.H.F. Well-studied Cu–BTC still serves surprises: Evidence for facile  $\text{Cu}^{2+}/\text{Cu}^+$  interchange. *Phys. Chem. Chem. Phys.* **2012**, *14*, 4383–4390. [[CrossRef](#)]
32. Fu, Q.; Xie, K.; Tan, S.; Ren, J.M.; Zhao, Q.; Webley, P.A.; Qiao, G.G. The use of reduced copper metal–organic frameworks to facilitate CuAAC click chemistry. *Chem. Commun.* **2016**, *52*, 12226–12229. [[CrossRef](#)]
33. Loera-Serna, S.; Oliver-Tolentino, M.A.; de Lourdes López-Núñez, M.; Santana-Cruz, A.; Guzmán-Vargas, A.; Cabrera-Sierra, R.; Beltrán, H.I.; Flores, J. Electrochemical behavior of  $[\text{Cu}_3(\text{BTC})_2]$  metal-organic framework: The effect of the method of synthesis. *J. Alloys Compd.* **2012**, *540*, 113–120. [[CrossRef](#)]
34. Dhumal, N.R.; Singh, M.P.; Anderson, J.A.; Kiefer, J.; Kim, H.J. Molecular Interactions of a Cu-Based Metal–Organic Framework with a Confined Imidazolium-Based Ionic Liquid: A Combined Density Functional Theory and Experimental Vibrational Spectroscopy Study. *J. Phys. Chem. C* **2016**, *120*, 3295–3304. [[CrossRef](#)]
35. Borfecchia, E.; Maurelli, S.; Gianolio, D.; Groppo, E.; Chiesa, M.; Bonino, F.; Lamberti, C. Insights into Adsorption of  $\text{NH}_3$  on HKUST-1 Metal–Organic Framework: A Multitechnique Approach. *J. Phys. Chem. C* **2012**, *116*, 19839–19850. [[CrossRef](#)]
36. Wen, L.-L.; Wang, F.; Feng, J.; Lv, K.-L.; Wang, C.-G.; Li, D.-F. Structures, Photoluminescence, and Photocatalytic Properties of Six New Metal–Organic Frameworks Based on Aromatic Polycarboxylate Acids and Rigid Imidazole-Based Synthons. *Cryst. Growth Des.* **2009**, *9*, 3581–3589. [[CrossRef](#)]
37. Wen, L.; Zhao, J.; Lv, K.; Wu, Y.; Deng, K.; Leng, X.; Li, D. Visible-Light-Driven Photocatalysts of Metal–Organic Frameworks Derived from Multi-Carboxylic Acid and Imidazole-Based Spacer. *Cryst. Growth Des.* **2012**, *12*, 1603–1612. [[CrossRef](#)]
38. Schlichte, K.; Kratzke, T.; Kaskel, S. Improved synthesis, thermal stability and catalytic properties of the metal-organic framework compound  $\text{Cu}_3(\text{BTC})_2$ . *Microporous Mesoporous Mater.* **2004**, *73*, 81–88. [[CrossRef](#)]
39. DeCoste, J.B.; Peterson, G.W.; Schindler, B.J.; Killops, K.L.; Browe, M.A.; Mahle, J.J. The effect of water adsorption on the structure of the carboxylate containing metal–organic frameworks Cu-BTC, Mg-MOF-74, and UiO-66. *J. Mater. Chem. A* **2013**, *1*, 11922–11932. [[CrossRef](#)]
40. Chen, X.; Mao, S.S. Titanium Dioxide Nanomaterials: Synthesis, Properties, Modifications, and Applications. *Chem. Rev.* **2007**, *107*, 2891–2959. [[CrossRef](#)]
41. Tranchemontagne, D.J.; Hunt, J.R.; Yaghi, O.M. Room temperature synthesis of metal-organic frameworks: MOF-5, MOF-74, MOF-177, MOF-199, and IRMOF-0. *Tetrahedron* **2008**, *64*, 8553–8557. [[CrossRef](#)]



© 2019 by the authors. Licensee MDPI, Basel, Switzerland. This article is an open access article distributed under the terms and conditions of the Creative Commons Attribution (CC BY) license (<http://creativecommons.org/licenses/by/4.0/>).